

# Electronic structures of intermetallic borides $RPd_3B_x$ ( $R$ =rare-earth metals)

C. Loison,\* A. Leithe-Jasper, and H. Rosner†

Max-Planck-Institut für Chemische Physik fester Stoffe, Nöthnitzer Straße 40, 01187 Dresden, Germany

(Received 13 October 2006; published 31 May 2007)

The electronic structure and the theoretical lattice parameters for the intermetallic antiperovskites  $RPd_3B$  ( $R$  from La to Yb) are calculated within the density-functional theory using the LSDA+ $U$  functional (LSDA is local spin density approximation) to include strong electronic correlations at the  $R$  site. Exemplarily, the electronic structure of  $LaPd_3B$  is discussed and compared with the isoelectronic and isostructural superconductor  $MgCNi_3$ . The coherent potential approximation is applied to calculate the lattice parameters of  $RPd_3B_x$ , where  $R=La$  and  $Lu$ , as a function of the boron content  $x$ . Contrarily to what was reported by Dhar *et al.* [Mater. Res. Bull. **16**, 1557 (1981)], a regular increase is observed in the whole range  $x \in [0, 1]$ . Moreover, the calculated lattice parameters obtained for the whole family  $RPd_3B$ , with  $R$  from La to Yb, are much higher than the experimental lattice parameters published by Dhar *et al.*, questioning their synthesis of stoichiometric compounds  $RPd_3B$ . Attempts to synthesize  $RPd_3B$  with  $R=La, Yb$  failed for  $LaPd_3B$ . Instead, in the case of exposure to air,  $LaPd_3O_x$  is obtained. On the contrary,  $YbPd_3B_x$  could be obtained ( $0 \leq x \leq 0.6$ ). For this phase, the LSDA+ $U$  calculations indicate a valence instability. Thus, boron insertion in  $RPd_3$  seems eased by the tendency of the rare earth to become divalent.

DOI: 10.1103/PhysRevB.75.205135

PACS number(s): 71.20.Eh, 71.15.Mb, 75.20.Hr

## I. INTRODUCTION

Antiperovskites  $MXT_3$  ( $M=Mg, Cu, La, \dots$ ,  $X=B, C, N$ , and  $T$  a transition metal) have the same structure as the perovskite  $CaTiO_3$ , except for the exchanged positions of the light atom and the transition metal. Among the family of antiperovskites, the superconductor  $MgCNi_3$  ( $T_c=8$  K) has received considerable attention (see Ref. 1 for a recent review). Due to the high amount of Ni, magnetic interactions are present in  $MgCNi_3$  and their influence on the superconductivity mechanism is not fully understood yet. It has been shown that  $MgCNi_3$  is near a ferromagnetic instability,<sup>2-4</sup> which can be reached, for example, by hole doping at the Mg site. Unfortunately, it has been impossible so far to investigate the effect of enhanced spin fluctuations on the superconductivity in doped compounds such as  $Mg_{1-x}Li_xCNi_3$  or  $Mg_{1-x}Na_xCNi_3$  because all attempts to prepare such samples failed.

Intermetallic antiperovskites closely related to  $MgCNi_3$  are therefore subject to investigations, both in the search for new superconductors and in the pursuit of a better understanding of the interplay between superconductivity and magnetism. It was suggested that boron-containing antiperovskites may be good candidates.<sup>5-7</sup>

$LaPd_3B$  is a particularly interesting representative of these boron-containing antiperovskites because it is isostructural and isoelectronic to  $MgCNi_3$ . Its synthesis has been reported by Dhar *et al.*,<sup>8</sup> but to our knowledge, neither its electronic nor its magnetic properties have been investigated yet. In the present work, the electronic structures of  $LaPd_3B$  and  $MgCNi_3$  are compared and the tendencies toward ferromagnetism or superconductivity are discussed. Since La itself carries no  $4f$  magnetic moment, replacing Ni by Pd should reduce the tendency toward magnetism in favor of superconductivity.  $LaPd_3B$  may be easier to hole dope than  $MgCNi_3$ ,<sup>7</sup> and one may expect a variety of electronic structures while changing the boron content and the rare-earth metal  $R$  from

lanthanum to lutetium. In fact, the whole row of  $RPd_3B_x$  shows interesting features, and the experimental data available on  $RPd_3B_x$  (Refs. 8–12) raised several questions.

(i) X-ray-diffraction (XRD) patterns of  $RPd_3B_x$  clearly indicate a cubic symmetry, but x-ray-absorption near-edge-structure (XANES) spectra of  $EuPd_3B_x$  lead to some discussion on the position of the boron.<sup>13</sup> This question is addressed in Sec. III A, where the two models for the crystal structure of  $RPd_3B_x$  are discussed. The results of our theoretical calculations strongly favor the classical antiperovskite picture.

(ii) Intriguingly, the experimental lattice parameter of  $LaPd_3B_x$  reported by Dhar *et al.* does not depend on the amount of boron.<sup>8</sup> For the other lanthanides, Dhar *et al.*<sup>8</sup> suggest that the lattice parameter of  $RPd_3B_x$  increases for low boron content ( $x \leq 0.3$ ) and saturates for  $0.5 \leq x$  or  $0.8 \leq x$ . In a different interpretation, the lattice parameter of  $RPd_3B_x$  increases almost linearly with the boron content  $x$  until the solubility limit of boron in the perovskite is reached.<sup>5,7,14</sup> Indeed, various solubility limits have been reported for different antiperovskite borides.<sup>5,15,16</sup> To clarify this question, Sec. III presents theoretical results on calculated lattice parameters of  $RPd_3B_x$  and Sec. IV presents the experimental results on  $YbPd_3B_x$  and  $LaPd_3B_x$ . Special care has been taken in the determination of the boron content.

(iii) Finally, the XANES and XRD spectra of  $EuPd_3B_x$  and  $CePd_3B_x$  (Refs. 6 and 9–12) indicate a transition in the valence state of europium or cerium when boron is inserted. Section III presents theoretical results on the valence of the lanthanide in  $RPd_3B_x$  for  $R$  from lanthanum to lutetium.

The present paper is organized as follows: In Sec. II, the theoretical and experimental methods are detailed. Section III is dedicated to theoretical results, while Sec. IV reports the experimental results. Finally, both experimental and theoretical data are comparatively discussed.

## II. METHODS

### A. Calculations details

We performed the electronic structure calculations using the density-functional theory within the local spin density approximation (LSDA) with the exchange and correlation functional proposed by Perdew and Wang.<sup>17</sup> The electronic structures have been obtained by the FPLO4.00 band-structure calculation code (full-potential nonorthogonal local Orbital<sup>18,19</sup>) using a minimum basis set including semicore, valence, and polarization orbitals:  $R(4f5s5p)(6s6p5d)$ ,  $B(2s2p3d)$ , and  $Pd(4s4p)(5s5p4d)$ . All these states are calculated self-consistently, the core state fully relativistically, and the semicore and valence states scalar relativistically. The long-range part of the Ewald summation was decomposed in 1000–2500 Fourier components. The  $k$  convergence of the total energy within  $10^{-4}$  hartree was achieved for  $24^3$   $k$  points in the full Brillouin zone.

The localized nature of  $f$  electrons and their subtle many-body effects are generally badly described by the LSDA functionals. The LSDA+ $U$  formalism in which a Hubbard-like interaction term is included for the  $f$  electrons is a mean-field approach to treat this problem. This approach has proven to be meaningful in investigating valence transitions in lanthanide compounds.<sup>20,21</sup> The two main parameters in the LSDA+ $U$  are the Hubbard  $U$  and the interatomic exchange  $J$ . They were treated as parameters,  $U$  was set to 7 eV [typical for the lanthanides<sup>22</sup> and consistent with x-ray-absorption near-edge-structure spectra of  $\text{EuPd}_3\text{B}_x$  (Ref. 11)] and  $J$  to 0. A change of  $U$  from 6 to 9 eV and  $J$  from 0 to 1 eV did not change our conclusions. The double counting term was chosen with the atomic limit.

For the calculations with nonstoichiometric  $\text{RPd}_3\text{B}_x$ , we have used the coherent potential approximation<sup>23–25</sup> (CPA) implemented in FPLO.<sup>19</sup> The calculations include an empty site E at the boron position to model  $\text{RPd}_3\text{B}_xE_{1-x}$ . The basis set for this empty site was  $(1s2p3d)$  without optimization of the FPLO compression factor.<sup>47</sup> For the ordered cases ( $x=0$  and  $x=1$ ), the CPA calculations were checked with usual ordered structure calculations using the Blackman-Esterling-Berk<sup>26</sup> potential. In order to evaluate the reliability of the CPA approach for these compounds, we applied it to the isostructural compound  $\text{ScRh}_3\text{B}_x$ , where experimental and theoretical data are well documented (see Sec. III C). Following FPLO4.00 notations, the basis set used was  $\text{Sc}(3s3p)(4s4p3d)$ ,  $\text{Rh}(4s4p)(5s5p4d)$ ,  $\text{B}1s(2s2p3d)$ ,  $\text{E}(1s2p3d)$ .

### B. Experimental methods

Samples were prepared from La and Yb (pieces, Hunan Rare Earth Metals Materials Company, 99.9 wt %; Ames 99.95 wt %), Pd (foil, Chempur, 99.95 wt %), and crystalline B (pieces, Chempur, 99.995 wt %). Master alloys of  $\text{Pd}_3\text{B}_x$  were arc-melted together with La metal. All manipulations were performed inside an argon filled glovebox ( $\text{O}_2$  and  $\text{H}_2\text{O}$  partial pressures lower than 1 ppm). For homogeneity annealing, each sample was welded inside a Ta ampoule which was then sealed in quartz ampoules and kept at 800 °C for

7 days followed by 10 days at 1000 °C. Finally, the ampoules were quenched in cold water. Due to the rather high volatility of Yb metal,  $\text{YbPd}_3\text{B}_x$  samples were prepared from Yb filings which were mixed with powdered  $\text{Pd}_3\text{B}_x$ , pressed into pellets, welded into Ta ampoules, slowly heated to 800 °C, and kept there for 2 days. After this prereaction step, the samples were arc-melted and subjected to homogenization annealing similar to the La-containing samples.

All samples were characterized by powder XRD performed on a HUBER G 670 imaging plate Guinier camera, equipped with a Ge monochromator and  $\text{Cu } K\alpha_1$  ( $\lambda = 1.54056 \text{ \AA}$ ) or  $\text{Co } K\alpha_1$  radiation ( $\lambda = 1.78901 \text{ \AA}$ ). For the powder XRD, the samples were crushed and powdered inside an argon-gas filled glovebox. The samples were then loaded between two polyimide foils in an aluminum holder with a rubber sealing to exclude air and moisture, and subjected to XRD analysis immediately afterward. The lattice parameters were refined by least-squares fitting of Guinier powder data with  $\text{LaB}_6$  as an internal standard,  $a = 4.15692(1) \text{ \AA}$ , by using WINXPOW (STOE) and the WINCSD program package.<sup>27</sup> For metallographic examination, pieces of about 3 mm diameter were cut from the annealed samples. They were embedded in an epoxy resin. Grinding was performed on abrasive papers (500 and 1000 grit silicon carbide) and an alcohol-based lubricant. Polishing was done using slurries of 9- and 3-micron diamond powder in alcohol-based lubricants. The microstructures were examined optically (Zeiss Axioplan 2) and with a scanning electron microscope (Philips SL 30). All experimental steps were carried out in an argon filled glovebox system. The compositions of the observed phases were analyzed by energy dispersive x-ray spectroscopy (Philips XL 30) and wavelength dispersive x-ray spectroscopy (Cameca SX 100) using  $\text{Pd}_5\text{B}_2$  as boron and palladium,  $\text{Yb}_3\text{Pd}$  as ytterbium, and  $\text{LaPt}_2$  as lanthanum standards. These standards were prepared as single phase materials and subjected to chemical analysis (inductively coupled plasma-optical emission spectroscopy). Chemical analysis on oxygen was carried out on a LECO TCH 600 hot gas extractor.

## III. THEORETICAL RESULTS

### A. Crystal structure

The structure of  $\text{RPd}_3$  belongs to the cubic  $\text{AuCu}_3$  type (space group  $Pm\bar{3}m$ , No. 221) with a lattice parameter slightly larger than 4 Å for all lanthanides. The rare-earth metal occupies the position 1a (0,0,0), the palladium the position 3c. In general, in  $\text{RPd}_3\text{B}_x$ , the boron insertion is at the position 1b ( $1/2, 1/2, 1/2$ ), leading to the  $\text{CaTiO}_3$  type of structure [see Fig. 1(a)]. For  $\text{EuPd}_3\text{B}_x$ , an alternative model with the boron in position 3d ( $1/2, 0, 0$ ) has been proposed [see Fig. 1(b)].<sup>13</sup> This second model has been inspired by Mössbauer spectra indicating a changing environment of the boron with the temperature. To estimate the most favorable structure, the total energies of the two models have been calculated and the lattice parameters optimized, keeping the cubic symmetry and the crystallographic positions fixed. Noticeably, in model B, the full stoichiometry  $\text{EuPd}_3\text{B}$  corre-

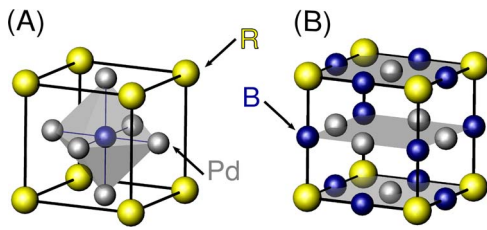


FIG. 1. (Color online) Two models for the cubic crystal structures of  $\text{EuPd}_3\text{B}$ : (A) with the boron in the center of the cell and (B) with the boron on the edge of the unit cell.

spond to a partial occupation of the 3d position by the boron. Using CPA calculations, we took into account the disorder due to the partial occupation but neglected the local distortions. The three equivalent (d) positions are then occupied by  $\text{B}_{1/3}\text{E}_{2/3}$ . Within these approximations, the energy of model A ( $a_0=4.29 \text{ \AA}$ ) is 3 eV lower than the one of model B ( $a_0=4.36 \text{ \AA}$ ). Such a high energy difference could not be compensated by local distortions, which energies are typically in the order of phonon energies and thus lower than a few hundred meV. Furthermore, the calculated lattice parameter for model B deviates even more from the experimental data.<sup>8</sup> Therefore, the following sections consider only model A.

### B. LSDA+ $U$ electronic structures

The influence of the Hubbard term on the electronic densities of states of  $\text{RPd}_3$  and  $\text{RPd}_3\text{B}$  is illustrated in Fig. 2. Considering the atomic configuration of erbium ( $4f^{12}, 6s^2$ ),

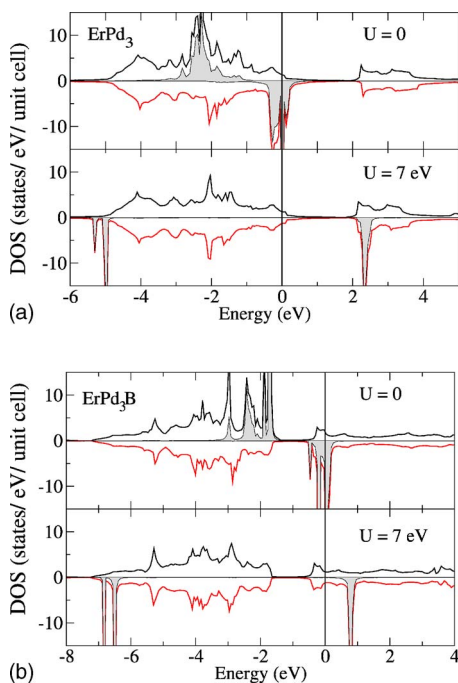


FIG. 2. (Color online) Electronic density of states of  $\text{ErPd}_3$  with lattice parameter  $a_0=4.03 \text{ \AA}$  and  $\text{ErPd}_3\text{B}$  with lattice parameter  $a_0=4.29 \text{ \AA}$ . The Fermi level is at 0. Positive DOS correspond to spin up, negative ones to spin down. The partial densities of  $f$  states are filled in gray.

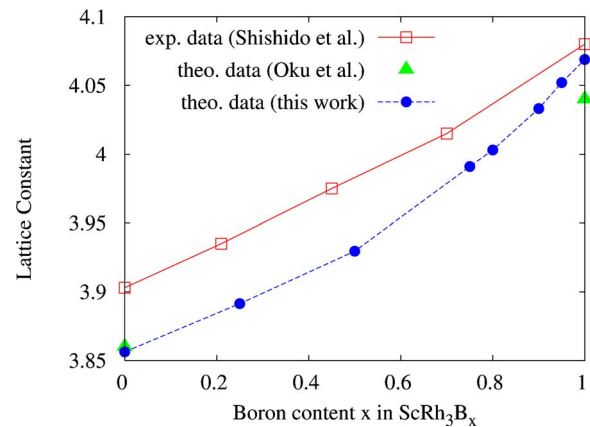


FIG. 3. (Color online) Lattice parameter of  $\text{ScRh}_3\text{B}_x$  as a function of  $x$ , in  $\text{Å}$ ; experimental results are from Ref. 16, while theoretical results are from Ref. 31 and from this work.

its  $4f$  shell is neither empty, half-filled, nor full, and is then typical for the lanthanide row.

In LSDA calculations,  $4f$  orbitals of erbium hybridize strongly with other bands, and some are located at the Fermi level. Non- $4f$  orbitals are also spin polarized. These results are typical for LSDA functionals, but not physically correct. With  $U=7 \text{ eV}$ , the fully occupied  $4f$  bands are shifted toward lower energies, and become invisible in Fig. 2. The partially occupied  $4f$  band which was located at the Fermi level is split into two peaks far from the Fermi level. They are approximately 7 eV apart, which corresponds as expected to the  $U$  value. The Hubbard term permits one to get the correct description of the system near the Fermi level, without any  $4f$  bands.<sup>28</sup>

Noticeably, the convergence of the calculations is sometimes difficult because of the valence instabilities. In some cases, the self-consistent LSDA+ $U$  solutions depend on the initial electronic density or on the convergence procedure.<sup>48</sup> This is a known problem of the method.<sup>28</sup> For example, a metastable self-consistent solution was obtained for  $\text{SmPd}_3$ : the  $4f$  states do not split at  $U=7 \text{ eV}$ , they are only broadened. Moreover, these  $4f$  states interact with the other states, and some of them remain at the Fermi level. Besides, non- $4f$  states are highly spin polarized. We considered a self-consistent solution as trustworthy if it fulfills the following criteria: (i) the  $4f$  density of states at the Fermi level is low,<sup>29,30</sup> (ii) the  $4f$  states are highly localized, and (iii) the spin polarization of non- $4f$  states is low. In fact, either all of these criteria were fulfilled, or none of them. Unfortunately, no solutions following these criteria could be obtained for  $\text{SmPd}_3$ ,  $\text{TbPd}_3$ ,  $\text{DyPd}_3$ , and  $\text{DyPd}_3\text{B}$ .

### C. Test of the CPA approach

The CPA approach was tested by calculating the evolution of the lattice parameter as a function of boron content for  $\text{ScRh}_3\text{B}_x$ . This compound is isostructural to  $\text{RPd}_3\text{B}_x$ , with similar atom types, and some experimental and theoretical data have been published already.<sup>16,31</sup> In this compound, the lattice parameter increases almost linearly with the amount of boron. As can be seen in Fig. 3, the theoretical lattice

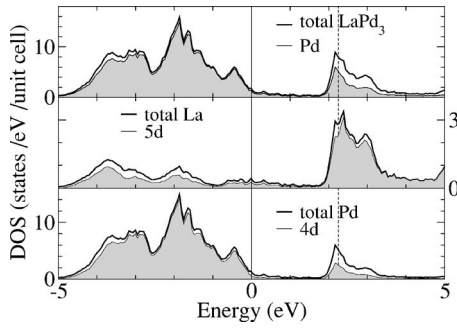


FIG. 4. Density of states and projected density of states of  $\text{LaPd}_3$ . The Fermi level is at 0. The vertical dotted line corresponds to the position of the Fermi level if three electrons were added within the rigid-band approximation.

parameters are 1%–2% lower than the experimental results in the whole range of composition. Such systematic deviation is well known for the LSDA. The application of CPA is thus well justified for the class of compounds investigated here. It was applied to distinguish between the two models of  $\text{EuPd}_3\text{B}$  (see Sec. III A) and to calculate the lattice parameters of  $\text{LaPd}_3\text{B}_x$  and  $\text{LuPd}_3\text{B}_x$  as a function of the boron content  $x$  (see Sec. III E).

#### D. $\text{LaPd}_3\text{B}$ compared to $\text{MgCNi}_3$

For  $\text{LaPd}_3\text{B}_x$ , no  $f$  electrons are present so that the results of the LSDA+ $U$  and LSDA calculations are very similar. According to our calculations, neither  $\text{LaPd}_3$  nor  $\text{LaPd}_3\text{B}$  are magnetic.

Figure 4 shows the density of states (DOS) and projected densities of states of  $\text{LaPd}_3$ . It shows principally two broad peaks, with a pseudogap of about 2 eV above the Fermi level. The broad valence band just below the Fermi level is mainly composed of palladium 4d states. The broad unoccupied band is a hybridization of both palladium ( $5s, 5p, 4d$ ) and lanthanum states (mostly 5d). In between, the density of states is uniformly low, without any singular shape around the Fermi level. Adding the three electrons of the boron within the rigid-band approximation would shift the Fermi level by about 2 eV (see the vertical dotted line in Fig. 4). However, Fig. 5 shows that the DOS of  $\text{LaPd}_3\text{B}$  is not just a rigid shift of the DOS of  $\text{LaPd}_3$ , because the boron 2s and 2p states hybridize with the two principal bands (grossly Pd 4d band and Pd+La d band). The DOS details are changed and, in particular, the Fermi level is situated just above a relatively narrow peak (Pd 4d, La 5d, and B 2p). In the case of only partial occupation of the B position, the Fermi energy would lie right in the pseudogap. In Fig. 6, the densities of states of  $\text{MgCNi}_3$  and  $\text{LaPd}_3\text{B}$  around the Fermi level are compared. Both structures show a relatively high peak near the Fermi level, and the density of states at the Fermi level is very similar. On the other hand, the peak of  $\text{LaPd}_3\text{B}$  is much further away from the Fermi level than  $\text{MgCNi}_3$  (0.25 eV compared to 0.06 eV) and it is broader. This difference may result in different magnetic behaviors of the two compounds. It was shown that  $\text{MgCNi}_3$  is close to itinerant magnetism<sup>2,3,32</sup> and should become ferromagnetic under Li

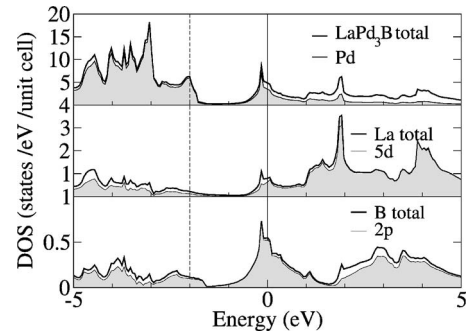


FIG. 5. Total density of states and projected densities of states of  $\text{LaPd}_3\text{B}$ . The Fermi level is at zero energy. The vertical dotted line corresponds to the position of the Fermi level if three electrons were removed within the rigid-band approximation.

doping.<sup>4</sup> With the exchange interaction  $I \sim 0.3$  eV of  $\text{MgCNi}_3$  and the sharp peak in the density of states very close to the Fermi level  $N(E_F)$ , the Stoner factor

$$S = \frac{\chi}{\chi_0} = \frac{1}{1 - N(E_F)I} \quad (1)$$

( $\chi$  is the observed magnetic susceptibility and  $\chi_0$  the Pauli susceptibility) diverges if the Fermi level is lowered by a few meV upon hole doping. For  $\text{LaPd}_3\text{B}$ , the exchange interaction  $I$  of Pd is expected to be considerably smaller than for Ni,<sup>33</sup> and the density of states at the Fermi level  $N(E_F)$  would not change much under doping. As a consequence, no magnetic effect is expected in  $\text{LaPd}_3\text{B}$ , even under hole doping.

To confirm this assumption, we investigated the effect of Sr doping by calculating the electronic structure of  $\text{La}_x\text{Sr}_{1-x}\text{Pd}_3\text{B}$  within virtual-crystal approximation.<sup>34</sup> In such calculations, one diminishes the number of valence electrons and the charge of La nucleus, mimicking Sr doping. In our case, for 73% of Sr, the Fermi level reaches the maximum of the DOS peak, which is even sharper than for pure  $\text{LaPd}_3\text{B}$ . However, even a density of states at the Fermi level as high as 10 states/eV/unit cell is not sufficient to induce ferromagnetic instability. The minimum of the total energy of  $\text{La}_x\text{Sr}_{1-x}\text{Pd}_3\text{B}$  for a spin moment of 0 was carefully checked using fixed-spin-moment calculations.

The superconductivity of  $\text{MgCNi}_3$  is due to the electron-phonon coupling for a rotating mode of the nickel

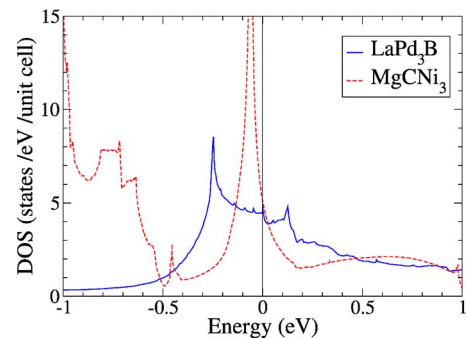


FIG. 6. (Color online) Electronic density of states of  $\text{LaPd}_3\text{B}$  and  $\text{MgCNi}_3$  ( $U=0$ ). The Fermi level is at zero energy.

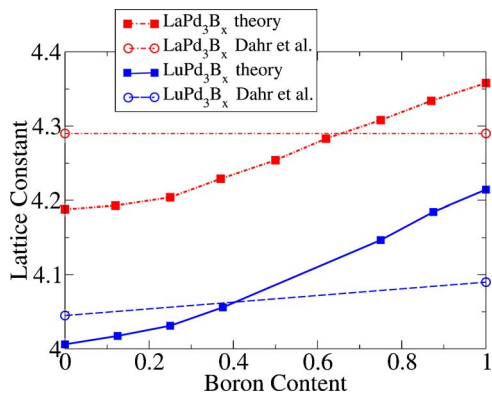


FIG. 7. (Color online) Lattice parameter (in Å) of  $RPd_3B_x$  ( $R = \text{La, Lu}$ ) as a function of  $x$ .

octahedra.<sup>2</sup> Such a strong coupling may be present in the isostructural and isoelectronic  $\text{LaPd}_3\text{B}$ . In this case, the suppression of the magnetic fluctuations in  $\text{LaPd}_3\text{B}$  relative to  $\text{MgCNi}_3$  may favor the appearance of a superconducting state.<sup>32</sup> These theoretical results stimulated us to prepare and investigate samples of  $\text{LaPd}_3\text{B}$ . Experimental results are presented in Sec. IV.

#### E. Lattice parameters upon boron insertion

In this section, the calculated lattice parameters of  $RPd_3$  and  $RPd_3\text{B}$  are discussed. The reported lattice parameters ( $a_0$ ) correspond to the minima of parabolic fits of the total energy as a function of  $a_0$  using about 10 values within  $\pm 5\%$  around the minimum.

We first discuss the theoretical results for La and Lu, which  $4f$  shells are either empty or full, so that no particular behavior due to  $f$  electrons is expected. The theoretical lattice parameters as a function of boron content of  $\text{LaPd}_3\text{B}_x$  and  $\text{LuPd}_3\text{B}_x$  are plotted in Fig. 7 with filled squares. The evolution is approximately linear in the range  $0.3 \leq x \leq 1$ , without any saturation for high  $x$ . These behaviors are very similar to the experimental and theoretical results obtained for  $\text{ScRh}_3\text{B}_x$ . However, they disagree with the experimental results published by Dhar *et al.* (empty circles). The difference of lattice parameters at  $x=1$  for  $\text{LaPd}_3\text{B}$  and  $\text{LuPd}_3\text{B}$  can be attributed neither to the LSDA (it underestimates  $a_0$ ) nor to the CPA treatment (in these ordered cases the usual calculations give the same results). The anomalously low value of the experimental lattice parameter suggests that the saturation of the lattice parameter observed experimentally is due to the limit of solubility of the boron in  $RPd_3$ .

For the other lanthanides, the lattice parameters were only calculated for  $x=0$  and  $x=1$ , but the conclusions are similar. Figure 8 compares the lattice parameter reported by Dhar *et al.* (circles) to the calculations (squares). For  $RPd_3$  (filled symbols), the calculated lattice parameters are a few percent smaller than the experimental ones, which is the typical underestimation obtained with LSDA calculations. The relative differences of lattice parameters found with  $U=0$  and  $U=7$  eV are less than 0.5%, even if the valence of the rare earth is not properly described with  $U=0$ . Additionally, the results of the calculations are in agreement with the lan-

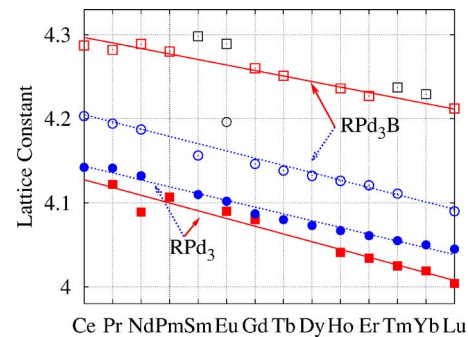


FIG. 8. (Color online) Lattice parameters (in Å) of  $RPd_3$  (filled symbols) and  $RPd_3\text{B}$  (empty symbols). The experimental data from Dhar *et al.* (Ref. 8) are plotted with open circles ( $RPd_3$ ) and filled circles ( $RPd_3\text{B}$ ). The calculated parameters are plotted with open squares ( $RPd_3$ ) and filled squares ( $RPd_3\text{B}$ ), respectively. Lines represent the linear fit for the lanthanide contraction rules. The divalent cases ( $\text{SmPd}_3\text{B}$ ,  $\text{EuPd}_3\text{B}$ ,  $\text{TmPd}_3\text{B}$ , and  $\text{YbPd}_3\text{B}$ , see Sec. III F), depicted by black symbols, were excluded for the fitting procedure.

thanide contraction, showing a linear decrease of the lattice parameter with the nucleus charge. For  $RPd_3\text{B}$ , the calculated lattice parameters are about 5% higher than the experimental ones. Such a discrepancy is not typical for the LSDA calculations, with or without the Hubbard  $U$ . Two interpretations may explain the discrepancy between the experimental and theoretical lattice parameters: (i) a substoichiometry in the synthesized compounds and (ii) mixed valence states which cannot be reproduced by the LSDA+ $U$  calculations. Both interpretations may be valid, depending on the rare earth. For  $\text{LaPd}_3\text{B}_x$  and  $\text{LuPd}_3\text{B}_x$ , a mixed valence state can be ruled out. In fact, for most of the lanthanide compounds no valence transition is expected upon boron insertion (see the next section for a detailed discussion). Thus, we suggest that the samples of Dhar *et al.* were substoichiometric, i.e., with  $x < 1$  (see also Sec. IV). This can be easily deduced from the experimentally observed variation of the lattice parameter with increasing boron content, which rises to certain values and keeps constant despite further boron addition. These findings can be explained in terms of solubility limits of boron incorporation in the  $RPd_3$  compounds well before the intended stoichiometric  $RPd_3\text{B}$  compositions are reached.

#### F. Valence transitions upon boron insertion

In solids, the rare earth metals mostly favor a trivalent state. In a simplified local orbital picture, the  $5d$  and  $6s$  of the rare earth participate at the conduction band, while the  $4f$  orbitals remain localized.<sup>35</sup> However, Ce and Sm, Eu, Yb, or Tm have been found also in tetravalent and divalent states, respectively, or in more complicated configurations such as mixed or intermediate valences.<sup>36–38</sup> In these states, the  $4f$  shell contains one electron more, and is for example, stabilized through a full or half-full state. The valence of the rare-earth metal depends therefore on the fine tuning between the energy of interaction between localized  $f$  electrons and the cohesive energy of more delocalized electrons participating to the conduction bands of the metals.<sup>29,30,39–41</sup>

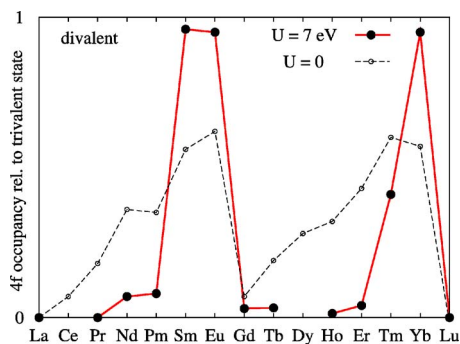


FIG. 9. (Color online) Occupation of the  $4f$  orbitals of  $RPd_3B$  relative to the trivalent case for  $U=0$  and  $U=7$  eV. The lattice parameter are optimized for each compound and are those plotted in Fig. 8.

An anomaly in the unit-cell volume of the compound relative to the lanthanide contraction rule for trivalent ions often points out an unusual valence state.<sup>8</sup> In the present case, both experimental results and our calculations clearly indicate an atypical behavior of  $EuPd_3B_x$  (see Fig. 8), which is interpreted as a tendency toward a mixed or divalent state. The valence state can be investigated in more detail by measuring the magnetic susceptibility, Mössbauer spectra,<sup>13,42</sup> or x-ray photoemission and x-ray-absorption spectra, respectively.<sup>38</sup> Experimental results show that the insertion of boron may have different effects on the valence state of the lanthanoid in  $RPd_3$ : though the valence of  $R$  seems to be unchanged for most of the compounds, for europium<sup>8</sup> and ytterbium, the addition of boron is followed by a change of valence from 3 to 2.  $EuPd_3$  also shows valence instabilities at surfaces.<sup>43</sup> On the contrary, the valence of cerium changes from a mixed valence state to a trivalent state.<sup>9,12,44,45</sup>

From the theoretical point of view, the valence can be deduced from the occupation number  $n_f$  of the  $4f$  orbitals. As the FPLO code uses local orbitals as a basis set, the occupation number is easy to define and is directly obtained during the calculation of the Kohn-Sham eigenstates. In this formulation,  $n_f$  depends only slightly on the optimized basis set, but with LSDA+ $U$ , they are close to an integer number  $n$  ( $|n_f - n| \leq 0.2$ ). The interpretation in terms of divalent or trivalent states is then unambiguous. Note that the present calculations base on the hypothesis of a homogeneous and unique valence for the rare earth. They do not model a mixed valence state, neither inhomogeneous nor dynamical. Therefore, the calculations give us the most stable among different integer valence states. For  $RPd_3$ , the occupancies reveal only trivalent ions. For  $RPd_3B$ , the occupation numbers of the  $4f$  relative to the trivalent state  $[n_f - (Z - 57)]$ , where  $Z$  is the nuclear charge] are plotted in Fig. 9: they vary from zero for the trivalent state to 1 for the divalent state. According to the LSDA+ $U$  calculations, most of the rare-earth metals are trivalent in  $RPd_3B$ . Clearly Sm, Eu, and Yb are divalent. The case of Tm is unclear. For Ce and Dy, we did not get any valid results (i.e., fulfilling our convergence criteria described in Sec. II). The results obtained with the LSDA ( $U=0$ ) are plotted for comparison. They give only a rough tendency of the valence of the rare earth, and the calculation yields unphysical electronic densities of states. This shows

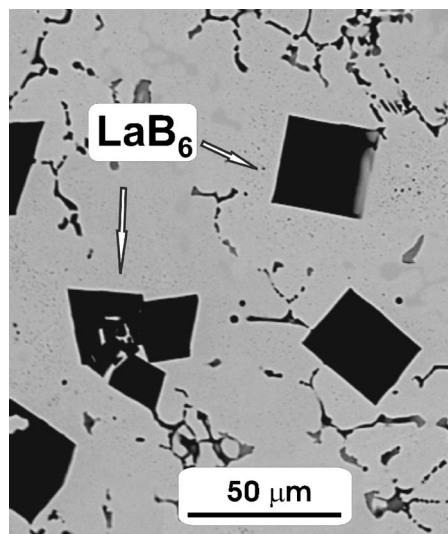


FIG. 10. Metallography picture of the results of the synthesis of  $LaPd_3B_{1-x}$ . Cubic crystals of  $LaB_6$  are embedded in a  $LaPd_3$  matrix.

again the necessity to use LSDA+ $U$  to treat the  $f$  states in this case. The LSDA+ $U$  calculations confirm the valence transition triggered by the boron insertion proposed for  $EuPd_3B_x$ . To our knowledge, no valence transition could yet be experimentally observed for  $SmPd_3B_x$  or  $YbPd_3B_x$ .

#### IV. EXPERIMENTAL RESULTS

In respect of such discrepancy between the observed and calculated lattice parameters, we have chosen  $LaPd_3$  and  $YbPd_3$  to investigate the boron incorporation experimentally.  $LaPd_3$  was selected since the valence fluctuating behavior of La can be ruled out and due to the fact that, according to results of Dhar *et al.*, the lattice parameter of  $LaPd_3B_x$  shows, in contrast to all other  $RPd_3B_x$  compounds, no increase with increasing amount of incorporated boron. Since the theoretical calculations predict a change in valence of Yb from trivalent Yb in  $YbPd_3$  to divalent Yb in  $YbPd_3B$ , we studied experimentally the boron uptake in  $YbPd_3$ . For this purpose, annealed samples were investigated by metallography and powder XRD.

*LaPd<sub>3</sub>B*. Several  $LaPd_3B_x$  samples with a nominally increasing boron content were synthesized. Due to the refractory nature of  $LaB_6$  ( $T_M=2715$  °C), direct synthesis from the elements was avoided in favor of the reaction of La metal with homogeneous prereacted  $Pd_3B_x$ . Metallographic analysis of the air sensitive materials revealed almost no incorporation of boron into the  $LaPd_3$  structure. Instead, formation of crystals of  $LaB_6$  embedded in a  $LaPd_3$  matrix could be observed (see Fig. 10). Despite the fact that all experimental steps were carried out in a glovebox, evaluation of the lattice parameters revealed a significant time-dependent lattice expansion (see Fig. 11). This can be explained by a slow diffusion of oxygen through the protective foil which covers the x-ray sample holder (see Sec. II B). This contamination with air obviously leads to incorporation of oxygen. The expansion of the cubic lattice proceeds from  $a=4.1861(2)$  Å for

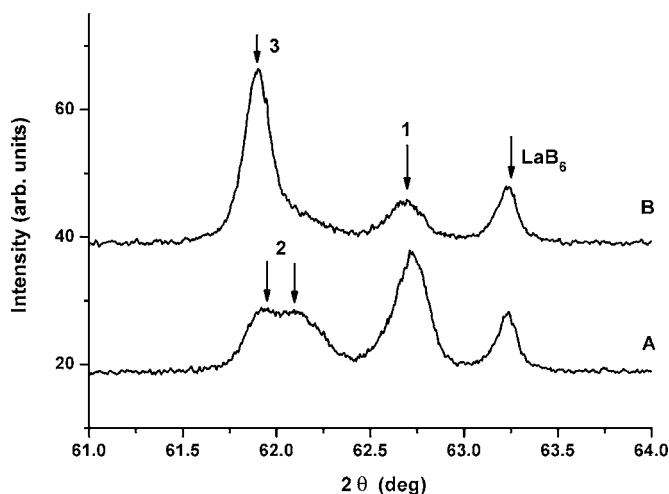


FIG. 11. Time-dependent evolution of the observed powder XRD pattern for  $\text{LaPd}_3$ . A, pattern taken after 10 min exposure time. Both cubic and tetragonal distorted phases I and II are seen (arrows 1 and 2). B, pattern taken after 90 min exposure time. Note the significant decrease in the content of the cubic phase I and transformation of the tetragonal intermediate phase II into cubic phase III (arrow 3) with enlarged lattice parameter. The Bragg (221) reflection of  $\text{LaB}_6$  which was used as internal standard is indicated.

the freshly prepared powder via a tetragonal distorted intermediate state [ $a, b = 4.2248(2)$ ,  $c = 4.2068(2)$ ] to  $a = 4.2368(2)$  Å found for samples which were exposed to air (see Fig. 12). Noticeably, the value for the oxidized sample corresponds to the value of the lattice parameter observed by Dhar *et al.*<sup>10</sup> Upon oxidation, the cubic volume expansion is

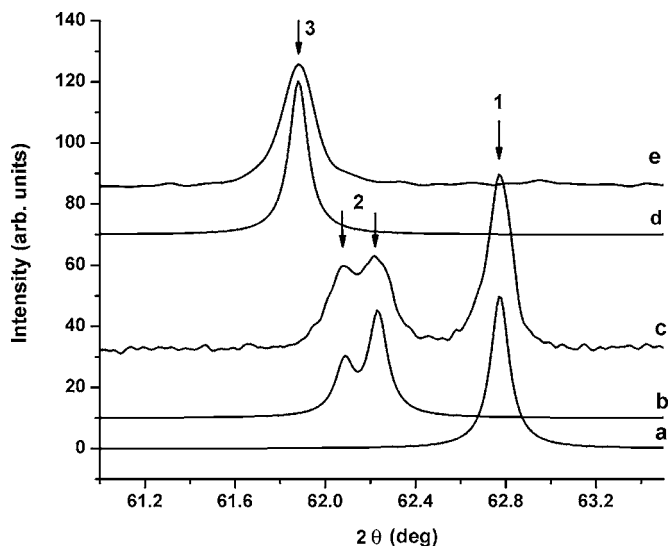


FIG. 12. Theoretical and observed powder XRD pattern for  $\text{LaPd}_3$ . a, theoretical pattern depicting the cubic (220) reflection for phase I (arrow 1); b, theoretical pattern depicting the tetragonal split (220) and (202) (arrows 2) reflections of intermediate phase II; c, observed pattern containing both cubic and tetragonal distorted phases I and II; d, Theoretical pattern depicting the cubic (220) reflection (arrow 3) for a cubic phase III with larger unit cell; and e, observed pattern containing the cubic phase III with enlarged lattice parameter.

about 3.7%. Besides the fundamental reflexes corresponding to the expanded cubic unit cell, several weak superstructure reflexes are observed which can be indexed based on a cubic unit cell with doubled lattice parameter.

Chemical analysis of these samples reveals an uptake of up to 1.5 wt % oxygen. A detailed investigation of the oxidation process will be published elsewhere. From these investigations, we can rule out a significant uptake of boron into  $\text{LaPd}_3$ . On the other hand,  $\text{LaPd}_3$  can be easily oxidized in air, which results in a slightly expanded lattice.

$\text{YbPd}_3\text{B}_x$ . In the case of the boron incorporated in  $\text{YbPd}_3$ , we could reach a maximum content of 11 at % boron which results in  $\text{YbPd}_{2.99(2)}\text{B}_{0.45(1)}$  with a cubic lattice parameter  $a = 4.0938(2)$  Å. Different from the La-containing samples, no formation of binary Yb borides (despite their refractory nature) as side products was detected. However, we observe a significant range of homogeneity for the binary compound  $\text{YbPd}_3$ , namely, from Pd-rich  $\text{YbPd}_{3.44(2)}$  [ $a = 4.0317(4)$  Å] to Yb-rich  $\text{YbPd}_{2.75(1)}$  [ $a = 4.0506(3)$  Å]. This binary homogeneity region, which is observed for many  $\text{RPd}_3$  compounds,<sup>46</sup> makes an evaluation of the degree of boron filling solely based on lattice parameter investigations difficult and questionable.

These results can be discussed by comparison to the experimental studies of Takeya and Shishido.<sup>15</sup> According to their experimental study concerning the homogeneity range of numerous intermetallic borides  $\text{RM}_3\text{B}_x$  (with  $R$  a rare earth, and  $M$  Rh, Pd, or Pt), the number of valence electrons per unit cell gives a good hint about the stability. For the stable compounds, this number is limited to the range from 31 to 34.5. With three valence electrons for the boron, the trivalent  $\text{RPd}_3\text{B}$  is stable for  $0 \leq x \leq 0.5$  and the divalent is stable in the range  $0.33 \leq x \leq 0.83$ . Similar observations were made in alkaline-earth metal based  $\text{MPd}_3\text{B}_x$  ( $M = \text{Mg}, \text{Ca}$ ),<sup>7</sup> where solubility limits of  $x = 0.71$  and  $x = 0.76$  for Mg and Ca, respectively, were found. This approach is only phenomenological, but it helps one to understand that the boron insertion is facilitated for compounds containing an electropositive metal which is or can become divalent, such as Mg, Ca, or Eu, Sm, and Yb. The insertion is much more difficult with La. We observed that the insertion of oxygen in  $\text{LaPd}_3$  also leads to a structural instability.

## V. SUMMARY

We have investigated experimentally and theoretically rare-earth intermetallic borides  $\text{RPd}_3\text{B}_x$  ( $R$  from La to Lu).

The electronic structure of hypothetical  $\text{LaPd}_3\text{B}$  was compared to the isoelectronic and isostructural superconductor  $\text{MgCNi}_3$ . A peak in the density of states is present at 0.4 eV below the Fermi level, but no itinerant magnetism is expected, even under hole doping. If the compound could be prepared, this suppression of magnetic fluctuations would favor superconductivity.

A critical reconsideration of experimental data<sup>8–10,13</sup> is proposed in the light of *ab initio* results. The CPA approach was first tested and then applied to calculate the lattice parameters of  $\text{LaPd}_3\text{B}_x$  and  $\text{LuPd}_3\text{B}_x$ , which increase almost linearly with the amount of boron in the whole range  $x$

$\in [0, 1]$ . These results disagree with the experimental data published by Dhar *et al.* Additionally, the present contribution includes the calculated lattice parameters of  $RPd_3$  and the stoichiometric  $RPd_3B$  for  $R$  from La to Lu. The lattice parameters are about 5% higher than what they measured. We suggest that the discrepancy may be explained by a sub-stoichiometry of some of their samples ( $x < 1$ ). On the other hand, the tendency to valence fluctuation observed experimentally for  $EuPd_3B_x$  (Refs. 10 and 11) is confirmed by the LSDA+ $U$  calculations.

We synthesized  $RPd_3B_x$  with  $R=La, Yb$  and investigated very precisely the homogeneity and boron content of the products.  $LaPd_3B$  could not be obtained with the standard

procedure.<sup>10,11</sup> Instead, in the case of exposure to air,  $LaPd_3O_x$  is obtained. We synthesized  $YbPd_3B_x$  for  $0 \leq x \leq 0.45$ . Further microprobe studies are required to elucidate this behavior in more detail.

#### ACKNOWLEDGMENTS

The DFG Emmy-Noether program (C.L. and H.R.) and the SFB 463 are acknowledged for financial support. We thank U. Burkhardt for metallography and electron microprobe analysis. The help of I. Veremchuk with the synthesis of  $YbPd_3B_x$  samples is acknowledged. We thank M. Richter, C. Geibel, and Yu. Grin for fruitful discussions.

\*Electronic address: loison@lasim.univ-lyon1.fr

†Electronic address: rosner@cpfs.mpg.de

<sup>1</sup>S. Mollah, *J. Phys.: Condens. Matter* **16**, R1237 (2004).

<sup>2</sup>D. J. Singh and I. I. Mazin, *Phys. Rev. B* **64**, 140507(R) (2001).

<sup>3</sup>S. Dugdale and T. Jarlborg, *Phys. Rev. B* **64**, 100508(R) (2001).

<sup>4</sup>H. Rosner, R. Weht, M. D. Johannes, W. Pickett, and E. Tosatti, *Phys. Rev. Lett.* **88**, 027001 (2001).

<sup>5</sup>H. Takei and T. Shishido, *J. Less-Common Met.* **97**, 223 (1984).

<sup>6</sup>C. Felser, *J. Alloys Compd.* **262-263**, 87 (1997).

<sup>7</sup>R. Schaak, M. Avdeev, W.-L. Lee, G. Lawes, J. Jorgensen, N. Ong, A. Ramirez, and R. Cava, *J. Solid State Chem.* **177**, 1244 (2004).

<sup>8</sup>S. Dhar, S. Malik, and R. Vijayaraghavan, *Mater. Res. Bull.* **16**, 1557 (1981).

<sup>9</sup>S. K. Dhar, S. K. Malik, and R. Vijayaraghavan, *Phys. Rev. B* **24**, 6182 (1981).

<sup>10</sup>S. Dhar, S. Malik, D. Rambabu, and R. Vijayaraghavan, *J. Appl. Phys.* **53**, 8077 (1982).

<sup>11</sup>B. Darshan, B. D. Padalia, R. Nagarajan, S. K. Dhar, S. K. Malik, and R. Vijayaraghavan, *Phys. Rev. B* **30**, 4031 (1984).

<sup>12</sup>M. Housiar, D. Adroja, and B. Rainford, *Physica B* **223-224**, 268 (1996).

<sup>13</sup>L. Cianchi, S. de Gennaro, F. Gulisano, M. Manchini, and G. Spina, *J. Phys.: Condens. Matter* **3**, 781 (1991).

<sup>14</sup>T. Shishido, J. Ye, T. Sasaki, R. Note, K. Obara, T. Takahashi, and T. Matsumoto, *J. Solid State Chem.* **133**, 82 (1997).

<sup>15</sup>H. Takeya and T. Shishido, *J. Less-Common Met.* **134**, 263 (1987).

<sup>16</sup>T. Shishido, J. Ye, S. Okada, K. Kudou, T. Sasaki, S. Isida, and T. Naka, M. Oku, I. Higashi, H. Kishi, H. Horiuchi, and T. Fukuda, *J. Alloys Compd.* **309**, 107 (2000).

<sup>17</sup>J. P. Perdew and Y. Wang, *Phys. Rev. B* **45**, 13244 (1992).

<sup>18</sup>K. Koepfner and H. Eschrig, *Phys. Rev. B* **59**, 1743 (1999).

<sup>19</sup>K. Koepfner, B. Velicky, R. Hayn, and H. Eschrig, *Phys. Rev. B* **55**, 5717 (1997).

<sup>20</sup>V. I. Anisimov, J. Zaanen, and O. K. Andersen, *Phys. Rev. B* **44**, 943 (1991).

<sup>21</sup>V. N. Antonov, B. N. Harmon, and A. N. Yaresko, *Phys. Rev. B* **72**, 085119 (2005).

<sup>22</sup>S. Hüfner and G. K. Wertheim, *Phys. Rev. B* **7**, 5086 (1973).

<sup>23</sup>P. Soven, *Phys. Rev.* **156**, 809 (1967).

<sup>24</sup>D. W. Taylor, *Phys. Rev.* **156**, 1017 (1967).

<sup>25</sup>B. Velick, S. Kirkpatrick, and H. Ehrenreich, *Phys. Rev.* **175**, 747 (1968).

<sup>26</sup>J. A. Blackman, D. M. Esterling, and N. F. Berk, *Phys. Rev. B* **4**, 2412 (1971).

<sup>27</sup>L. G. Akselrud, P. Y. Zavalii, Y. N. Grin, V. K. Pecharsky, B. Baumgartner, and E. Wölfel, *Mater. Sci. Forum* **133-136**, 335 (1993).

<sup>28</sup>H. J. Gotsis and I. I. Mazin, *Phys. Rev. B* **68**, 224427 (2003).

<sup>29</sup>P. Strange, A. Savane, W. Temmerman, and Z. Szotek, *Nature (London)* **399**, 756 (1999).

<sup>30</sup>W. Temmerman, A. Svane, P. Strange, Z. Szotek, and H. Winter, *Philos. Mag. B* **80**, 1179 (2000).

<sup>31</sup>M. Oku, T. Shishido, T. Shinohara, T. Fukuda, Q. Sun, Y. Kawazoe, and K. Wagatsuma, *J. Alloys Compd.* **339**, 317 (2002).

<sup>32</sup>L. Shan, Z. Y. Liu, Z. A. Ren, G. C. Che, and H. H. Wen, *Phys. Rev. B* **71**, 144516 (2005).

<sup>33</sup>P. Mohn, *Magnetism in the Solid State* (Springer, Berlin, 2003).

<sup>34</sup>L. Nordheim, *Ann. Phys.* **9**, 607 (1931).

<sup>35</sup>B. Johansson, *Phys. Rev. B* **20**, 1315 (1979).

<sup>36</sup>J. Kappler, M. Besnus, P. Lehmann, and A. Meyer, *J. Less-Common Met.* **111**, 261 (1985).

<sup>37</sup>R. Vijayaragharan, *J. Magn. Magn. Mater.* **47-48**, 561 (1985).

<sup>38</sup>T. Ito, A. Chainani, H. Kumigashira, T. Takahashi, and N. K. Sato, *Phys. Rev. B* **65**, 155202 (2002).

<sup>39</sup>A. Svane, *Phys. Rev. Lett.* **72**, 1248 (1994).

<sup>40</sup>A. Delin, L. Fast, B. Johansson, J. M. Wills, and O. Eriksson, *Phys. Rev. Lett.* **79**, 4637 (1997).

<sup>41</sup>L. Petit, S. Svane, P. Strange, H. Winter, and W. Temmerman, *J. Phys.: Condens. Matter* **13**, 8697 (2001).

<sup>42</sup>J. M. Cadogan, *J. Phys. D* **29**, 2246 (1996).

<sup>43</sup>G. Kaindl, G. Kalkowski, W. Brewer, B. Persheid, and F. Holtberg, *J. Appl. Phys.* **55**, 1910 (1984).

<sup>44</sup>Z. Szotek, W. M. Temmerman, and H. Winter, *Phys. Rev. Lett.* **72**, 1244 (1994).

<sup>45</sup>J. Kappler, M. Besnus, E. Beaurepaire, A. Mayer, J. Sereni, and G. Nieva, *J. Magn. Magn. Mater.* **47-48**, 111 (1985).

<sup>46</sup>T. B. Massalski, *Binary Alloy Phase Diagrams*, 2nd ed. (ASM International, Materials Park, OH, 2003).

<sup>47</sup>The basis optimization was accelerated and stabilized by grouping the orbitals in the following way:  $R:4f(5s5p)/(6s6p5d)+$ ,  $B:/(2s2p3d)+$ ,  $Pd:4s4p/(5s5p4d)+5d$ ,  $E:(1s2p)/+;$  number of Fourier components for the electrostatic part: at least 2500;

number of  $k$  points:  $16 \times 16 \times 16$ ; number of Fourier components for the electrostatic part: at least 2500; divisions for the overlap integrals meshes: radial 70, angular 28; confinement potential coefficient: 6; SC iteration with linear progress control (mixing=0.3); number of loops (SEI options): 50; number of energy points (SEI options): 30; lowest energy (SEI options): -2.0. Note that we first used the basis set obtained without CPA, and reoptimized the basis set only after a first convergence of the

density. Finally, when an empty state was used, the compression factor  $x_0$  of its orbitals ( $1s2p3d$ ) was kept fixed.

<sup>48</sup>For the problematic cases, we have first calculated the density with fixed spin moment (with several spin moments), and then relaxed the spin. For HoPd<sub>3</sub>B, TmPd<sub>3</sub>B, TbPd<sub>3</sub>, TmPd<sub>3</sub>, PmPd<sub>3</sub>, and PrPd<sub>3</sub>, we have first generated a fictitious solution with a high  $U$  (15 eV), and then diminished in a few steps the value of  $U$  to 7 eV.